Geochemistry, Geophysics, Geosystems

RESEARCH ARTICLE
10.1029/2019GC008514

Ge/Si Partitioning in Igneous Systems: Constraints From Laser Ablation ICP-MS Measurements on Natural Samples

Detao He[1,2], Cin-Ty A. Lee[2], Xun Yu[2,3], and Michael Farner[2]

[1]State Key Laboratory of Geological Processes and Mineral Resources, School of Earth Sciences, China University of Geosciences, Wuhan, China, [2]Department of Earth Science, Rice University, Houston, TX, USA, [3]State Key Laboratory of Marine Geology, Tongji University, Shanghai, China

Key Points:
- Mineral/melt and intermineral Ge/Si exchange coefficients for nine common rock-forming silicate minerals were determined
- Ge/Si exchange coefficients can vary by up to a factor of 10
- Ge/Si evolution process of MORB can be well modeled

Supporting Information:
- Supporting Information S1
- Data Set S1
- Data Set S2

Correspondence to:
D. He and C.-T. A. Lee,
detaohe@hotmail.com;
ctlee@rice.edu

Citation:
He, D., Lee, C.-T. A., Yu, X., & Farner, M. (2019). Ge/Si partitioning in igneous systems: Constraints from laser ablation ICP-MS measurements on natural samples. *Geochemistry, Geophysics, Geosystems*, *20*. https://doi.org/10.1029/2019GC008514

Received 19 JUN 2019
Accepted 23 AUG 2019
Accepted article online 11 SEP 2019

Abstract Mineral/melt and intermineral Ge/Si exchange coefficients for nine common rock-forming silicate minerals were determined by Laser Ablation Inductively Coupled Plasma Mass Spectrometry (LA-ICP-MS). Ge/Si mineral/melt exchange coefficients were found to vary by up to a factor of 10. In mafic and ultramafic systems, Ge/Si mineral/melt exchange coefficients are less than 1 for plagioclase (0.48) and olivine (0.72), close to 1 for clinopyroxene (1.17) and orthopyroxene (1.07), and greater than 1 for garnet (2.69). In felsic and silicic systems, the Ge/Si mineral/melt exchange coefficient is less than 1 for quartz (0.23), plagioclase (0.67), and potassium feldspar (0.67) but much greater than 1 for biotite (4.80) and hornblende (3.95). We show that early, olivine-dominated fractionation of primitive basalts does not fractionate Ge/Si significantly, but subsequent cotectic crystallization of plagioclase and pyroxene can increase the Ge/Si ratio from 6×10^{-6} to 7×10^{-6}. We show that the only way to decrease Ge/Si during magmatic differentiation is by crystallization of hornblende or biotite (though biotite is typically a late crystallizing phase), consistent with hornblende being a major fractionating phase in hydrous intermediate magmas. The high compatibility of Ge in hornblende makes this element, in conjunction with Si, a potentially useful approach for distinguishing between hornblende and garnet in the source regions of intermediate magmas. The high compatibility of Ge in micas suggests that Ge/Si systematics may also be useful in understanding the origin of ultrapotassic magmas, which are often thought to derive from phlogopite-rich sources.

1. Introduction

Few studies have been performed on Ge in rocks because it is generally thought that Ge behaves like Si, whose behavior is already well understood, and because of its low natural abundance (e.g., Arevalo et al., 2011; De Argollo & Schilling, 1978b; Derry et al., 2006; Kurtz et al., 2002; Le Roux et al., 2011; Wasson & Baedecker, 1970). Burton et al. (1959) systematically reported Ge abundance in over 200 terrestrial materials. Bernstein (1985), in a review of Ge geochemistry and mineralogy, showed that the Ge content of most terrestrial silicate rocks and common rock-forming silicate minerals are similar (from 1 to 4 ppm; Figure 1), but Ge in some sulfides and iron oxides can vary over several orders of magnitude. Ge and Si are thought to behave similarly because they have similar ionic radius, valence, and ionic potential under conditions typical of the Earth's crust and upper mantle (Ringwood, 1955). Thus, the Ge/Si ratio should be difficult to fractionate during melting or crystallization; that is, the Ge/Si mineral/melt exchange coefficient

$$K^{Ge/Si} = \frac{\left(C^{Ge}_{min}/C^{Si}_{min}\right)}{\left(C^{Ge}_{melt}/C^{Si}_{melt}\right)} \quad (1)$$

is approximately unity for many mineral/melt systems (Malvin & Drake, 1987), where C represents the concentration of a particular element in a given phase (mineral or melt). Minerals in which Ge and Si likely behave similarly are olivine and pyroxene (Capobianco & Watson, 1982; Malvin & Drake, 1987), the primary constituents of peridotitic mantle.

In detail, however, K is not unity. The Ge/Si mineral/melt exchange coefficient may deviate slightly from unity for such minerals as garnet, hornblende, and mica. In other cases, Ge's behavior can deviate substantially from that of Si. Ge has a strong preference for clay minerals, such that pelitic sediments become enriched in Ge relative to Si (Anders et al., 2003; Derry et al., 2006; Hammond et al., 2004; Kurtz et al.,

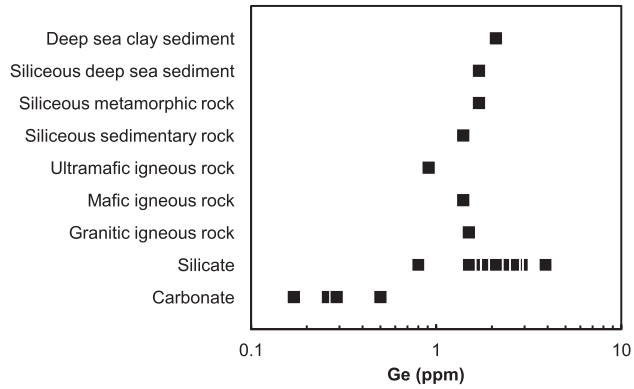

Figure 1. Ge content of various types of rocks and minerals. Data are from Bernstein (1985) and references therein.

2002; Lugolobi et al., 2010). Ge can be enriched in sulfide minerals (e.g., argyrodite, briartite, renierite, and germanite), sometimes to levels high enough to form Ge ore (Bernstein, 1985; Höll et al., 2007). Ge is also known to form complexes with organic molecules, which may decouple it from Si in some parts of the marine environment (Bareille et al., 1998; Dong et al., 2015; Shen et al., 2011; Tribovillard et al., 2011). Ge compounds are more volatile than Si compounds at high pressures in hot water vapor (Höll et al., 2007), which leads to the enrichment of Ge in hydrothermal minerals, such as topaz (Breiter et al., 2013). Finally, under high-temperature reducing conditions, such as during core-mantle segregation, Ge tends to be more metallic than Si at a given oxygen fugacity (e.g., Kegler & Holzheid, 2011; Righter et al., 2011). Altogether, some processes likely leave an imprint of fractionated Ge/Si ratio in various Earth materials whereas others, such as melting of peridotitic mantle, may not.

Another property of Ge that may make it a useful tracer of petrogenetic processes is that in silicate systems, Ge and Si are moderately incompatible to compatible; that is, the elemental exchange coefficient K is ~1. Ge concentrations, like Si concentrations in igneous rocks, are within a factor of 2. Ge is ~1.1 ppm in peridotitic mantle (McDonough & Sun, 1995) and ~1.3 ppm for continental crust (Rudnick & Gao, 2003). Element ratios based on moderately incompatible element systems are "buffered" by mineralogy and are thus difficult to disturb by contamination with small amounts of fluids or melts. The Ge/Si system becomes interesting when the petrogenetic process involves a mineral whose K deviates from unity. For example, recent studies by Le Roux et al. (2010) showed that Zn and Fe are moderately compatible and behave nearly identically during melting of the Earth's mantle under typical oxygen fugacities of the mantle, but their behaviors diverge when high oxygen fugacities, garnet, or high-temperature volatilization of Zn are involved.

Our goal is thus to develop a comprehensive set of accurate Ge/Si exchange coefficients in silicate systems so that we can identify when Ge/Si systematics can be used as a diagnostic tracer. The most recent attempts to quantify Ge/Si behavior have come from doped high-pressure, high-temperature experiments (Davis et al., 2013; Le Roux et al., 2011), but so far, there has been no systematic study of partitioning in natural samples, largely because of the low natural abundance of Ge and the difficulty of measuring Ge in situ. Recently, laser ablation coupled with high mass resolution magnetic sector inductively coupled plasma mass spectrometry (ICP-MS; Arevalo et al., 2011; Righter et al., 2011) has eased the accurate determination of Ge because of the high sensitivity and high mass resolving power of magnetic sector instruments, the latter essential for resolving the various mass interferences that seem to plague Ge in ICP-MS, such as $^{148}Sm^{2+}$, $^{148}Nd^{2+}$ on ^{74}Ge. Several experimental studies had reported the Ge partition coefficients for sporadic minerals (Davis et al., 2013; Le Roux et al., 2011, 2015). In this paper, we use natural samples to infer exchange coefficients, providing systematic Ge/Si exchange coefficients database for rock-forming silicate minerals in igneous systems. Although obtaining partition coefficients by nature phenocryst-matrix pairs encounter some challenges, our comprehensive set of Ge/Si exchange coefficients can be used interrogate the origin and petrogenesis of some igneous rocks.

2. Sample and Methods

2.1. Samples

We analyzed mineral phases or lava groundmass in the following samples: spinel peridotite xenoliths from Samoa Island (SAM-03, SAM-04, SAM05, SAM-08, SAM-09) and Oak Creek lava flow in California, USA (OK98-98-3 and OK98-9; Lee et al., 2001); garnet peridotite xenoliths from Letlhakane kimberlite in Botswana (LETH3) and the Venetia kimberlite in South Africa (VEN1 and VEN2); garnet pyroxenites from Big Creek in California, USA (08BC16, 08BC17, 08BC19, 08BC20, 08BC26A, 08BC27-A, BC24B, BC76, BC98-1, and BC98-7; Chin et al., 2014; Lee et al., 2012; Lee et al., 2006); a plagioclase-phyric andesite from Mount Hood in Oregon, USA (L10MH20); granitic plutonic rocks from the Bernasconi Hills pluton in California, USA (213E1 and 214H1; Farner et al., 2014); tonalitic plutonic rocks from the Domenigoni Valley pluton in California, USA (2009 T-7; Liao et al., 2013); alkali basalts from Mount Trumbull in Arizona, USA (MT13A

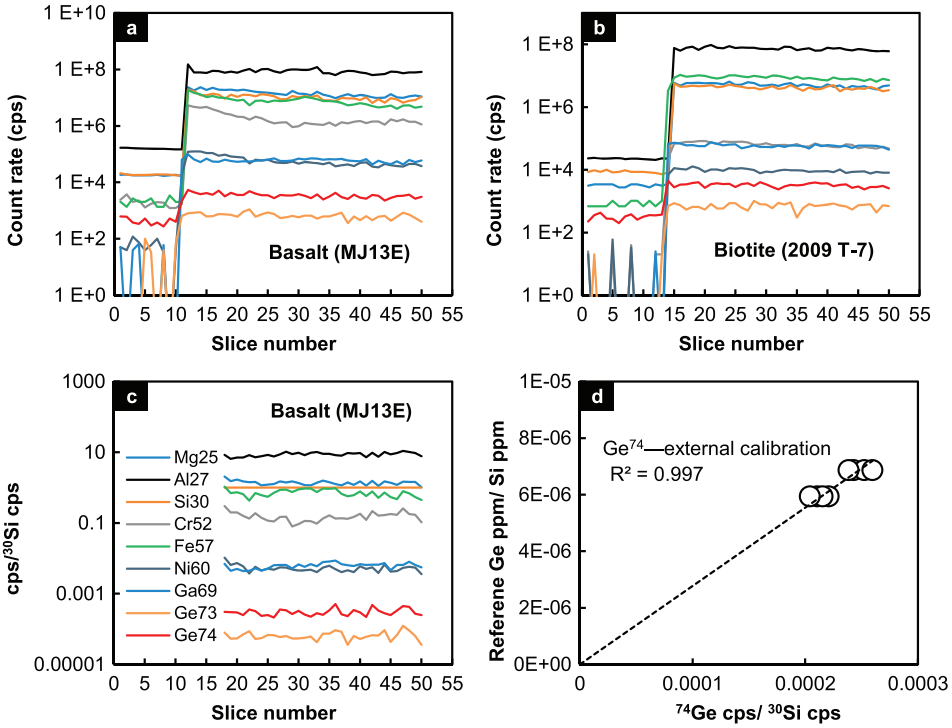

Figure 2. (a and b) Example of a time-resolved signal for laser ablation inductively coupled plasma mass spectrometry, including background and sample analysis. (c) Example of internal standard-normalized elemental signals after subtracting background for same sample as in Figure 2a. Parallel nature of each isotope signal implies homogeneity on the length scales of ablation. (d) External calibration curve of Ge^{74}.

and MT13E); alkali basalt from the Owens Valley in California, USA (AR); and ultrapotassic basalts from the San Joaquin volcanic field in the Sierra Nevada, California, USA (DS107A, M33, M72B, M73, MA102, MJ13E, H98A, and DY1; Van Kooten, 1980).

2.2. Analytical Methods

In situ analyses were obtained by laser ablation ICP-MS at Rice University using a Thermo Finnigan Element II Sector ICP-MS coupled with a New Wave 213 nm laser ablation system. Ablation was performed on ~150-μm-thick sections under a pure He atmosphere. Spot sizes of 110 μm were used in order to maximize sensitivity and homogenize large areas of fine-grained basalt and andesite groundmass. Laser energy density ranged between 11 and 15 J/cm^2, and the repetition pulse rate was set at 10 Hz. Analyses were carried out in medium mass resolution mode ($m/\Delta m$ = 3,000) in order to distinguish isobaric interferences on Ge masses (e.g., 73 and 74), although trace $^{58}Fe^{16}O^+$ and $^{36}Ar^{38}Ar^+$ on ^{74}Ge is still irresolvable. Sensitivity was typically estimated at about 200,000 cps (MR mode) for La on a BHVO-2g glass standard for a 55-μm, 10-Hz spot (15.6 ppm of La; Gao et al., 2002). Both ^{73}Ge and ^{74}Ge were monitored. Both gave the same concentration to within error, but because the isotope abundance and signal for ^{74}Ge is higher, we used ^{74}Ge to calculate Ge concentration. We also analyzed the following masses: ^{23}Na, ^{25}Mg, ^{27}Al, ^{30}Si, ^{31}P, ^{39}K, ^{44}Ca, ^{45}Sc, ^{48}Ti, ^{51}V, ^{52}Cr, ^{55}Mn, ^{57}Fe, ^{59}Co, ^{60}Ni, ^{63}Cu, ^{66}Zn, ^{69}Ga, ^{73}Ge, ^{74}Ge, ^{88}Sr, ^{89}Y, and ^{91}Zr (Dong et al., 2015; Shen et al., 2011). Analyses typically consisted of 10 measurements of gas background and 40 measurements during ablation of the sample (Figures 2a–2c). The ^{74}Ge intensities of background are 200–500 cps, while the sample signals are 5–30 times higher than background based on different type of mineral or rocks (Figures 2a and 2b). Gas background was averaged and then subtracted from ablation signal. Drift associated with ablation yield or matrix effects were controlled by internal normalization using ^{30}Si. U.S. Geological Survey glass standards BHVO-2g, BCR-2g, and BIR-1g were used as simultaneous external standards for all elements (Gao et al., 2002). The simultaneous use of several calibration standards helps to bracket the concentrations in the sample unknowns, decreasing errors associated with matrix-dependent elemental

fractionations and extrapolation of calibration curve (Lee et al., 2008). The accuracy of the external calibrations for Ge is shown in Figure 2d. Major and trace element concentrations on a volatile-free basis were estimated by assuming all the measured major elements as oxides (Na_2O, MgO, Al_2O_3, SiO_2, P_2O_5, K_2O, CaO, TiO, Cr_2O_3, MnO, and FeO) and then summing up to 100% (Lee et al., 2008; Liu et al., 2008; Shu & Lee, 2015). The external reproducibility and accuracy of the measurements were checked using U.S. Geological Survey standards BHVO-2g, BCR-2g and BIR-1g (Gao et al., 2002). For each analysis, the detection limit was estimated at 3 times the standard deviation of the background divided by the sensitivity. Additional details of analytical procedures are given in Lee et al. (2008) and Shu and Lee (2015).

3. Results

3.1. Ge/Si Systematics

3.1.1. Basalts

The basalt samples from three localities consist of >100-μm scale olivine phenocrysts set within an aphyric, microcrystalline groundmass, while two basalt samples (DY1 and H98A) contain plagioclase phenocrysts. In all cases, groundmass crystals are less than 30 μm. Our 110-μm-diameter spot size is larger than average grain size in the microcrystalline groundmass, but heterogeneities in the bulk composition of the groundmass still persist. This can be seen from the variability in Ge/Si ratio for different 110-μm laser ablation sampling of the basalt groundmass. This variation in measured Ge/Si ratio varies with MgO and Al_2O_3 due to variations in the abundance of microcrystalline clinopyroxene (Cpx) and plagioclase (Pl) that were not fully homogenized by a 110-μm spot size. We assumed that our sampling bias was random so that the average of numerous ablation spots provides the best estimate of the actual groundmass composition. For olivine (Ol) and plagioclase phenocrysts within the basalt, we analyzed several grains in each sample to obtain representative concentrations.

The Ge concentration (ppm by weight) and Ge/Si ratio (ppm/ppm) of basaltic groundmass and olivine phenocrysts are shown in Figure 3a and Tables S1 and S2 in the supporting information. Ge concentration of basaltic groundmass ranges from 1.4 to 2.1 ppm and Ge/Si ratio varies from 5.9×10^{-6} to 9.7×10^{-6}. Olivine phenocrysts have slightly lower Ge concentration (0.9 to 1.3 ppm) and Ge/Si ratio (5.1×10^{-6} to 6.6×10^{-6}) than the basalt groundmass. Ge content of plagioclase phenocrysts is about 0.8 ppm and Ge/Si ratio varies from 2.9×10^{-6} to 3.2×10^{-6}.

3.1.2. Peridotites

Seven spinel peridotite xenoliths and three garnet peridotite xenoliths from several place (see section 2.1) were used to study the Ge/Si partitioning coefficients. The spinel peridotites have clinopyroxene-orthopyroxene equilibration temperatures of ~1000 °C, while the garnet (Gt) peridotites equilibrated between 1000 and 1400 °C (Lee et al., 2001). Olivine has the lowest Ge/Si ratio (2.5×10^{-6} to 4.6×10^{-6}) and Ge concentration (0.5 to 0.9 ppm; $n = 23$) among the silicate phases (Tables S1 and S2). No significant difference was observed between olivines in spinel peridotite and in garnet peridotite. Clinopyroxene and orthopyroxene (Opx) have similar and moderate Ge concentration and Ge/Si ratio (Figure 3b and Tables S1 and 2). Ge content of orthopyroxene ranges from 1.3 to 1.8 ppm and Ge/Si ratio varies from 4.7×10^{-6} to 6.3×10^{-6} ($n = 10$). Ge content of clinopyroxene ranges from 1.2 to 1.5 ppm, and Ge/Si ratio varies from 4.7×10^{-6} to 6.3×10^{-6} ($n = 14$). Garnet has the highest Ge concentration (2.3 to 2.4 ppm) and the highest Ge/Si ratio (10.6×10^{-6} to 11.3×10^{-6}; $n = 3$) of the silicate minerals in peridotite (Tables S1 and S2). Spinel has the lowest Ge concentration (0.13 to 0.17 ppm; $n = 2$) and therefore contributes negligibly to the Ge and Ge/Si systematics of the bulk peridotite.

3.1.3. Garnet Pyroxenites

The garnet pyroxenites are dominated by clinopyroxene and garnet with lesser amounts of orthopyroxene, occasional amphibole. The garnet pyroxenites record equilibration temperatures below 900 °C (Lee et al., 2006). In general, garnets have much higher Ge contents and Ge/Si ratios than clinopyroxene (Figure 3c). Ge content of clinopyroxene ranges from 1.3 to 1.6 ppm, and Ge/Si ratio varies from 4.9×10^{-6} to 6.2×10^{-6} ($n = 8$), while Ge content of garnet ranges from 2.8 to 3.3 ppm and Ge/Si ratio varies from 14.2×10^{-6} to 15.8×10^{-6} ($n = 8$; Tables S1 and S2).

3.1.4. Andesites

An andesite from Mount Hood Oregon was used to study the Ge/Si exchange coefficients between plagioclase and melt. The mineral assemblage of the andesite is dominated by plagioclase and orthopyroxene

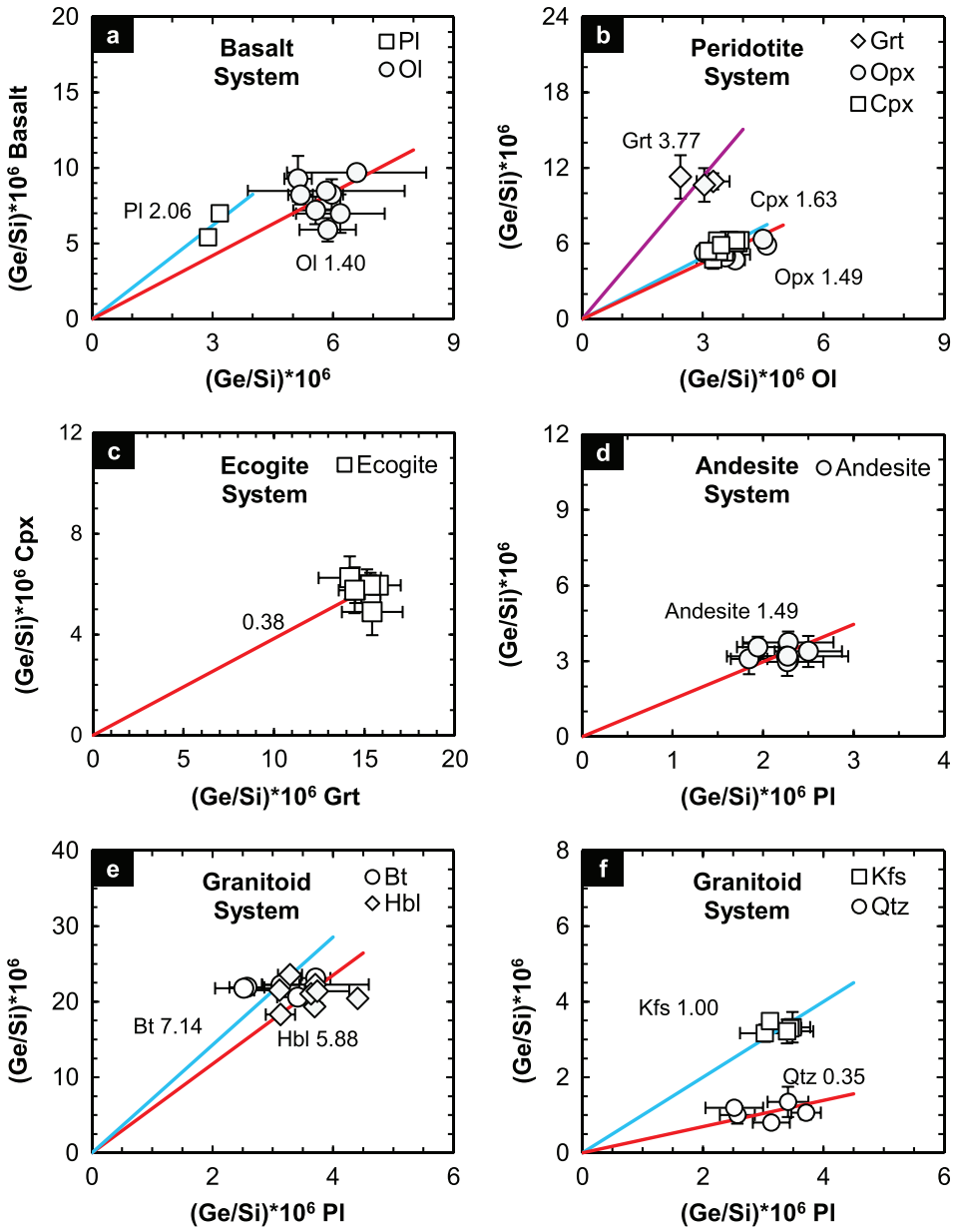

Figure 3. Ge/Si ratios of various minerals plotted against each other. Intermineral and mineral-melt exchange coefficients are calculated from the slope of linear regression lines forced through zero (orthogonal regression was assumed). Numbers within the plot represent the calculated slopes.

with minor clinopyroxene. We analyzed eight plagioclase phenocrysts and adjacent andesite groundmass pairs in thin section. For each plagioclase phenocryst-groundmass pair, we analyzed three spots to obtain a representative composition. Andesite has lower Ge and Ge/Si than basalt (Tables S1 and S2). The Ge content of andesite groundmass ranges from 1.0 to 1.2 ppm, and Ge/Si varies from 3.0×10^{-6} to 3.8×10^{-6} ($n = 8$). Plagioclase phenocrysts within andesite have lower Ge and Ge/Si compared to andesite groundmass (Figure 3d). Ge content of plagioclase phenocryst ranges from 0.5 to 0.7 ppm, and Ge/Si varies from 1.9×10^{-6} to 2.5×10^{-6} ($n = 8$; Tables S1 and S2), lower than that in the granites and diorites.

3.1.5. Granites and Diorites

In situ laser ablation ICP-MS analyses on minerals in two granites are shown in Table S1. We measured biotite (Bt), quartz (Qtz), potassium feldspar (Kfs), and plagioclase. In a given sample, biotite contains the highest Ge (~3.8 ppm) and Ge/Si (~22×10^{-6}) while quartz contains the lowest Ge (~0.5 ppm) and

Ge/Si (~1.1 × 10^{-6}). Plagioclase and potassium feldspar have almost the same Ge (~1.0 ppm) and Ge/Si (~3.3 × 10^{-6}; Figure 3f).

A diorite sample, biotite-rich (30%), and containing hornblende (~25%), plagioclase (~10%) and quartz (~35%) was analyzed to calculate the hornblende (Hb) and plagioclase Ge/Si exchange coefficient. Hornblende has much higher Ge (~4.3 ppm) and Ge/Si (~21 × 10^{-6}) than those (Ge ~ 1.0 ppm; Ge/Si ~ 3.3 × 10^{-6}) of plagioclase (Figure 3e).

4. Discussion

4.1. Intermineral and Mineral-Melt Exchange Coefficients

As stated in section 1, we define here the Ge/Si exchange coefficient ($K^{Ge/Si}$) between two phases *i* and *j* as

$$K^{Ge/Si} = \frac{\left(C_i^{Ge}/C_i^{Si}\right)}{\left(C_j^{Ge}/C_j^{Si}\right)} \quad (2)$$

C is concentration of Ge or Si in phase *i* or *j*. If the exchange coefficient of a given mineral pair is constant, then the Ge/Si ratios of two phases plotted on a binary plot will lie on an array that will project through the origin. The slope of this array is the exchange coefficient *K*. While the exchange coefficient will depend on temperature and the major element chemistry of the phases, we assume that the temperature dependence of Ge and Si partitioning are similar so that the exchange coefficient is less temperature sensitive. For example, Fe^{2+}/Mg^{2+} exchange coefficients are known to be relatively temperature-insensitive even though Fe and Mg partitioning are temperature sensitive (see Beattie et al., 1991). We thus forced a regression through zero to obtain exchange coefficients (Figure 3). This approach was used to obtain exchange coefficients from natural samples in Le Roux et al. (2010), which was then confirmed experimentally by Le Roux et al. (2015).

Intermineral exchange coefficients are reported in Table 1. It can be seen that exchange coefficients for a given mineral pair are, in some cases, identical within error, even for different systems. For example, the clinopyroxene-garnet exchange coefficient in high-temperature (>1200 °C) peridotite (0.43) is indistinguishable from that of eclogites (0.38), which equilibrated at lower temperatures (<900 °C). This suggests that temperature effects are canceled out (to within the error of our measurements) when considering Ge-Si exchange in mafic and ultramafic systems, even though Ge and Si partitioning individually depends on temperature.

Mineral-melt exchange coefficients are determined directly and indirectly. We are able to directly determine olivine/melt and plagioclase/melt exchange coefficients from phenocryst-lava groundmass pairs. The remaining mineral/melt exchange coefficients were determined by bootstrapping intermineral exchange coefficients. For example, the clinopyroxene/melt exchange coefficient is determined by multiplying the clinopyroxene/olivine by the olivine/melt exchange coefficient, $K^{Ge/Si}_{Cpx/melt} = K^{Ge/Si}_{Cpx/Ol} * K^{Ge/Si}_{Ol/melt}$. This approach of using natural samples was well demonstrated in Lee et al. (2012) for Cu and Le Roux et al. (2010) for Zn and Fe, again confirmed experimentally (Le Roux et al., 2011, 2015; Liu et al., 2014). Mineral/melt exchange coefficients calculated in this way are listed in Table 1.

We now compare our results to previous studies. The first systematic study on Ge partitioning in mafic systems was done experimentally in doped (1 wt. % levels of GeO_2) systems by Malvin and Drake (1987) with Ge determined by electron probe microanalysis. They obtain a Ge/Si exchange coefficient for olivine/melt of 0.73, clinopyroxene/melt of 1.4 and plagioclase/melt of 0.58 (Table 1). Despite the fact that their experiments were doped at concentrations 10^4 times that of natural systems used in the present study, our data agree with their results: Our exchange coefficient for olivine/melt is indistinguishable and those for clinopyroxene/melt and plagioclase/melt are ~17% and 16% lower than those of Malvin and Drake (1987), likely within error of measurements. Le Roux et al. (2011, 2015) also report Ge partition coefficients based on doped experiments in mafic systems. Our exchange coefficients for clinopyroxene/melt and olivine/melt are indistinguishable, and those for orthopyroxene/melt is 15% higher than those of Le Roux et al. (2011, 2015). Yang et al. (2015) reported the Ge content of Martian shergottites and olivine, orthopyroxene within it, yielding a Ge/Si exchange coefficient for olivine/melt of 0.75 and orthopyroxene/melt of 1.29. Our

Table 1
Intermineral and Mineral-Melt Exchange Partition Coefficients

Mafic system		Felsic system	
Intermineral exchange partition coefficients in mafic/felsic system			
$K_{Cpx/Ol}$	1.63 ± 0.03	$K_{Hb/Pl}$	5.88 ± 0.30
$K_{Opx/Ol}$	1.49 ± 0.06	$K_{Bt/Pl}$	7.14 ± 0.53
$K_{Gt/Ol}$	3.77 ± 0.36	$K_{Qtz/Pl}$	0.35 ± 0.04
$K_{Cpx/Grt}$	0.38 ± 0.01	$K_{Kfs/Pl}$	1.00 ± 0.03

Mafic system					Felsic system		
Mineral-melt exchange partition coefficients in mafic/felsic system							
	This study		M&D	Le Roux	Davis		Our data	Macdonald
$K_{Ol/Basalt}$	0.72	±0.04	0.73	0.79	0.43	$K_{Pl/Andesite}$	0.67	
$K_{Pl/Basalt}$	0.48	±0.02	0.58			$K_{Kfs/Andesite}$	0.67	0.21
$K_{Cpx/Basalt}$	1.17	±0.08	1.40	1.08	0.72	$K_{Hb/Andesite}$	3.96	3.41
$K_{Opx/Basalt}$	1.07	±0.08		0.93	0.70	$K_{Bt/Andesite}$	4.69	3.64
$K_{Gt/Basalt}$	2.69	±0.31			1.56	$K_{Qtz/Andesite}$	0.23	

Note. Data source: M&D: Malvin and Drake (1987); Le Roux: Le Roux et al. (2011, 2015); Davis: Davis et al. (2013); and Macdonald: Macdonald et al. (2007). Ol: olivine; Opx: orthopyroxene; Cpx: clinopyroxene; Gt: garnet; Hb: hornblende; Qtz: quartz; Kfs: potassium feldspar; Bt: biotite; Pl: plagioclase.

exchange coefficient for olivine/melt is indistinguishable, and those for orthopyroxene/melt are 17% lower than those of Yang et al. (2015). Davis et al. (2013) obtain Ge/Si exchange coefficients for olivine/melt of 0.43, clinopyroxene/melt of 0.72, orthopyroxene/melt of 0.70, and garnet/melt of 1.56 (Table 1). Our exchange coefficients are all about 60% higher than those of Davis et al. (2013) for reasons unknown, but as we will show below Ge/Si exchange coefficients of olivine and pyroxene closer to unity more readily explain natural mantle and mid-ocean ridge samples.

Independent constraints on Ge partitioning in felsic systems are sparse (Macdonald et al., 2007). The study of Macdonald et al. (2007) on natural rhyolite-phenocryst systems yield a Ge/Si exchange coefficient for hornblende/melt of 3.41, alkali feldspar/melt of 0.21, and biotite/melt of 3.64 (Table 1). Our exchange coefficients for hornblende/melt and biotite/melt in andesitic systems agree to within error with those of Macdonald et al. (2007), but our exchange coefficient for alkali feldspar/melt is twice that of Macdonald et al. (2007). We will show below, however, that our exchange coefficients can readily explain bulk rock data.

4.2. Bulk Peridotite/Melt Exchange Coefficients

The bulk peridotite/melt exchange coefficient $K^{Ge/Si}_{peridotite/melt}$ can be estimated from the measured olivine/melt exchange coefficient $K^{Ge/Si}_{Ol/melt}$ along with measured intermineral exchange coefficients, mineral modes in peridotite, and Si contents of each phase:

$$K^{Ge/Si}_{Peridotite/melt} = K^{Ge/Si}_{Ol/melt}\left[X^{Si}_{Ol} + X^{Si}_{Opx}K^{Ge/Si}_{Opx/Ol} + X^{Si}_{Cpx}K^{Ge/Si}_{Cpx/Ol} + X^{Si}_{Gt}K^{Ge/Si}_{Grt/Ol} + X^{Si}_{Sp}K^{Ge/Si}_{Sp/Ol}\right] \quad (3)$$

where $X^{Si}_j = C^{Si}_j x_j / C^{Si}_{peridotite}$ is the mass fraction of Si in phase j relative to the whole-rock (and C^{Si}_j and $C^{Si}_{peridotite}$ represent the concentration of Si in phase j and the bulk rock and x_j is the weight fraction of phase j in the rock). Thus, we can calculate the peridotite/melt Ge/Si exchange coefficient by assuming typical Si contents in peridotitic minerals and their mineral modes. We estimated bulk exchange coefficients for fertile spinel, fertile garnet peridotite, oceanic, and cratonic peridotite. The peridotite/melt Ge/Si exchange coefficients and mineral modes (Pearson et al., 2014; Walter, 1998, 2014; Workman & Hart, 2005) are reported in Table 2. Spinel has a negligible influence on bulk exchange coefficient owing to its low abundance. Clinopyroxene and orthopyroxene both have Ge/Si exchange coefficients near unity and thus have little impact on fractionation of Ge/Si. Instead, the Ge/Si exchange coefficients for peridotite/melt are mainly controlled by the proportions of olivine and garnet because Ge is mildly incompatible in olivine but compatible in garnet. Over the range of typical fertile upper mantle

Table 2
Peridotite/Melt Exchange Partition Coefficients of Ge/Si

	Modal Abundances in peridotites						
	Source of data[a]	Ol	Opx	Cpx	Sp	Gt	$K_{peridotite}$
Oceanic mantle peridotite	1	57	28	13	2		0.93
Fertile spinel peridotite	2	49.4	27.6	19.8	3.3		0.94
Fertile garnet peridotite	3	53.6	5.6	27.9		12.9	1.11
Craton peridotite	4	71.9	20.8	3.3	1.1	6.2	0.94

Note. Ol = olivine; Opx = orthopyroxene; Cpx = clinopyroxene; Sp = spinel; Gt = garnet; $K_{peridotite} = K^{Ge/Si}_{D(Peridotite/melt)}$.
[a]Mineral modes of mantle peridotites are from 1: Workman and Hart (2005); 2: Walter (2014); 3: Walter (1998); and 4: Pearson et al. (2014).

peridotite compositions, the bulk peridotite/melt Ge/Si exchange coefficient ranges from 0.93 to 1.11 from spinel- to garnet-facies peridotites, indicating that Ge/Si ratio of mantle-derived melts only change slightly relative to the mantle (Wasson & Baedecker, 1970).

4.3. Ge/Si Systematics in Basaltic Systems

4.3.1. Mid-ocean Ridge Basalts

Ge and Si data from mid-ocean ridge basalts (MORBs; Jenner & O'Neill, 2012; Yang et al., 2018) show that Ge/Si correlates negatively with MgO content (Figure 4a). To understand the evolution of Ge/Si in MORB during crystallization, we modeled fractional crystallization using thermodynamic programs (Asimow & Ghiorso, 1998; Ghiorso & Sack, 1995). We used pMELTS (Ghiorso et al., 2002) to calculate the major element composition of primary MORB, starting with a fertile mantle composition (Palme & O'Neill, 2014) having a Ge/Si ratio of $R^s_0 = 5.45 \times 10^{-6}$ (McDonough & Sun, 1995; Palme & O'Neill, 2014). We assumed isentropic

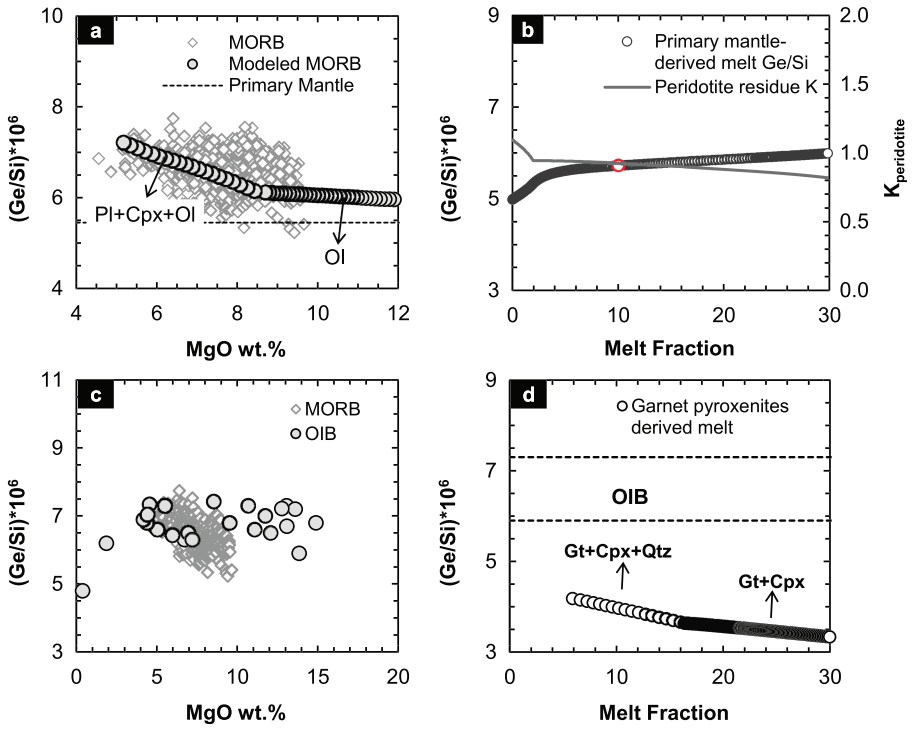

Figure 4. (a) Ge/Si versus MgO in mid-ocean ridge basalt (MORB; Jenner & O'Neill, 2012; Yang et al., 2018). Open squares represent modeled fractional crystallization liquid lines of descent (Asimow & Ghiorso, 1998; Ghiorso & Sack, 1995) with Ge/Si exchange coefficients determined in this study. (b) The modeled Ge/Si of melt derived from primary mantle. (c) Plot of Ge/Si versus MgO in ocean island basalts (OIBs), as represented by Hawaii based on data are from (De Argollo & Schilling, 1978a). (d) Ge/Si ratio of partial melts derived from remelting of MORB-like garnet pyroxenites in the eclogite stability field.

fractional melting (representing polybaric decompression melting) with a 1350 °C potential temperature and used a 10% aggregate melt to represent primary MORB. Ge systematics were modeled as follows. At every increment i of melting, melt Ge/Si ratio was calculated using

$$R_{i+1}^{m} = \frac{\mathrm{R}_{i+1}^{S}}{K_{i+1}^{s}} \tag{4}$$

where

$$R_{i+1}^{s} = \frac{\mathrm{R}_{i}^{s}\times\mathrm{C}_{i}^{s} - \mathrm{R}_{i}^{m}\times X_i\times\mathrm{C}_{i}^{m}}{\mathrm{C}_{i}^{s} - X_i\times\mathrm{C}_{i}^{m}} \tag{5}$$

R_i^m is the Ge/Si ratio of each melt increment, C_i^m and C_i^s are the Si concentration of each melt increment (m) and peridotite (s), X_i is the mass proportion of each melt increment relative to the peridotite residue, and K_{i+1}^S represents the Ge/Si exchange coefficient between bulk solid phases and melt, which changes as the mineral modes change (see equation (3)). We then integrate the melt increments to get an aggregate melt composition; we show how aggregate melt Ge/Si ratio varies as a function of melting degree (Figure 4b). It can be seen that Ge/Si is minimally fractionated (about 1.1 times) during peridotite melting. A typical melt derived from primary mantle (melt fraction of 10%) was used as the parental magma from which MORBs derive (parental MORB thus estimated to have a Ge/Si ratio of 5.72×10^{-6}).

We then used MELTS (Asimow & Ghiorso, 1998; Ghiorso & Sack, 1995) to model the differentiation of MORB. We allowed the parental, primary MORB to fractionally crystallize at 0.3 GPa. Si was tracked as an output from the MELTS program. The Ge/Si ratio of MORB at each increment of crystallization was determined using

$$R_{i+1}^{m} = \frac{R_{i}^{m}\times\mathrm{C}_{i}^{m} - K_{i}^{s}\times\mathrm{R}_{i}^{m}\times X_i\times\mathrm{C}_{i}^{s}}{\mathrm{C}_{i}^{m} - X_i\times\mathrm{C}_{i}^{s}} \tag{6}$$

where R_i^m and R_{i+1}^m represent the Ge/Si ratio of melt at increment i and $i + 1$, C_i^m and C_i^s represent the Si concentration of melt and bulk crystallized solid phases at each increment, K_i^s represents the Ge/Si exchange coefficient between bulk crystallized solid phases and melt, R_0^m is the parental MORB Ge/Si ratio, and X_i represents the mass proportion of crystallized solid phases at each increment. Results are shown in Figure 4a. It can be seen that our Ge/Si exchange coefficients, coupled with the MELTs thermodynamic models, reproduce the observed MORB Ge/Si systematics. For the first ~27% of crystallization, the liquid line of descent is controlled by olivine with a bulk Ge/Si exchange coefficient of 0.72. During this stage, MgO decreases rapidly while Ge/Si ratio increases gradually. Beyond ~27% crystallization, the melt undergoes cotectic crystallization with proportions of Pl, Cpx, and Ol, which altogether yield a higher but still incompatible bulk Ge/Si ratio exchange coefficient (about 0.74–0.83). Since the rate of decrease of MgO declines (because of plagioclase crystallization), the Ge/Si ratio increases more significantly with decreasing MgO in a Ge/Si-MgO diagram.

4.3.2. Ocean Island Basalts

There are limited studies on the Ge/Si systematics of ocean island basalts (OIBs). As far as we know, the only published data are those from Hawaiian volcanic rocks (De Argollo & Schilling, 1978a; Huang & Humayun, 2016). Unlike MORB, Hawaiian volcanic rocks do not show a clear trend between Ge/Si and MgO, although it would be worth remeasuring such data using more modern analytical tools with higher precision. In any case, Hawaiian volcanic rocks ($5.9–7.3 \times 10^{-6}$) fall within the same Ge/Si range as MORBs (Figure 4c). It has been suggested that pyroxenites might be present in OIB sources (e.g., Allègre & Turcotte, 1986; Dasgupta et al., 2010; Hirschmann et al., 2003; Sobolev et al., 2007), so the question arises as to whether the pyroxenites are influencing the Ge/Si of OIBs?

To evaluate the influence of pyroxenites during OIB genesis, we used pMELTS to model the Ge/Si ratio of melt derived from MORB-like garnet pyroxenites (Ghiorso et al., 2002). Since melts derived from pyroxenites are more silicic, more viscous and hence less mobile, such melts would be difficult to segregate at low melt fractions. For these reasons, we assumed isobaric (3.0 GPa) batch melting. An average MORB composition

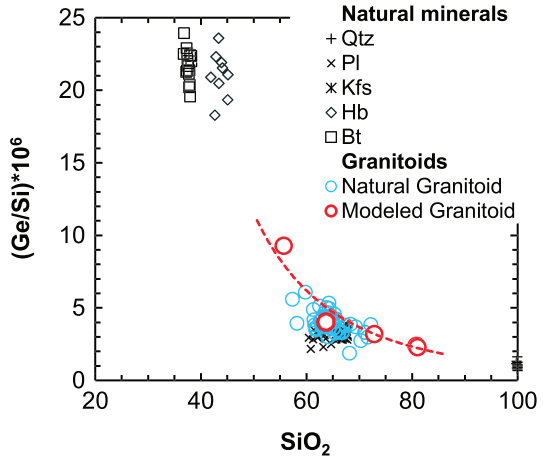

Figure 5. Ge/Si versus SiO_2 (wt. %) for granitoids and minerals within them. Granitoid data are from (Ayuso et al., 2009; Kamei & Takagi, 2003). Red circles represent model granitoid compositions based on mass balance of measured mineral compositions with mineral modes taken from Le Maitre et al. (2002). Qtz = quartz; Hb = hornblende; Pl = plagioclase; Kfs = alkali feldspar; Bt = biotite.

from Jenner and O'Neill (2012) was assumed. The Ge/Si ratios of melts can be easily calculated from the equation: $R^m = \frac{R^S}{K^S}$, where R^m and R^S are the Ge/Si ratio of melt and the solid garnet pyroxenite respectively and K^S is the bulk garnet pyroxenite/melt exchange coefficient. Importantly, because of garnet, Ge is compatible relative to Si; that is, K^S varies from 1.54 to 1.94 over the course of melting. Model melts derived from garnet pyroxenites thus have Ge/Si ratios from 3.3–4.2 × 10^{-6}, which is much lower than that of Hawaii (Figure 4d). Because Hawaii has similar Ge/Si ratio as MORB, this could imply that garnet pyroxenite may not be an important component in the mantle source region of Hawaii or more complex modeling of a pyroxenite melting, that is, with melt-rock reaction, might be necessary. We note, however, that Hawaii may not be representative of OIBs and the accuracy of existing Ge data of Hawaiian basalts might need reevaluation, so more work is necessary. We also have not explored the possibility of garnet pyroxenites having higher initial Ge/Si, compensating for the compatible nature of Ge during melting. Garnet pyroxenites formed as primary cumulates in arcs, where garnet is a liquidus phase, may have higher Ge/Si than garnet pyroxenites formed by metamorphism of MORBs, which never saw any significant garnet fractionation.

4.4. Granitoid Ge/Si Ratio

The major minerals in granitoids are quartz, plagioclase, alkali feldspar, biotite, and hornblende. As shown in Figure 5, granitoids have Ge/Si ratio less than that of MORBs (Ayuso et al., 2009; Kamei & Takagi, 2003). They also define a rough trend of Ge/Si decreasing with increasing SiO_2. We did not attempt to model the Ge/Si of granitoid formation using MELTS or related thermodynamic programs because of their difficulty in predicting amphibole and biotite proportions. We can nevertheless show that granitoid Ge/Si systematics can be readily explained as a mass balance between these different minerals:

$$R^{Ge/Si}_{Granitoid} = \frac{X_{Qtz}\times C^{Ge}_{Qtz} + X_{Pl}\times C^{Ge}_{Pl} + X_{Kfs}\times C^{Ge}_{Kfs} + X_{Bt}\times C^{Ge}_{Bt} + X_{Hbl}\times C^{Ge}_{Hbl}}{X_{Qtz}\times C^{Si}_{Qtz} + X_{Pl}\times C^{Si}_{Pl} + X_{Kfs}\times C^{Si}_{Kfs} + X_{Bt}\times C^{Si}_{Bt} + X_{Hbl}\times C^{Si}_{Hbl}} \quad (7)$$

where $R^{Ge/Si}_{Granitoid}$ is the Ge/Si of the granitoid, $X_{mineral}$ is the mineral mode, and $C^{Ge}_{mineral}$ and $C^{Si}_{mineral}$ are the typical Ge and Si concentrations of each mineral phase. The mineral modes of several kinds of granitoids (granite, granodiorite, monzonite, and diorite; Le Maitre, 2002) and typical Ge and Si contents of each mineral (Table 3) were used to model the Ge/Si ratio of granitoid as weighted averages of the mineral phases (Figure 5). Modeled granitoids define a curved mixing (or unmixing) trend line in Ge/Si versus SiO_2 space, with Ge/Si decreasing with increasing SiO_2. Our models predict that the Ge/Si ratio of granitoids should be less than that of basalts, primarily due to fractionation of hornblende. Although hornblende is not an early fractionating phase of hydrous basalts, the presence of primary hornblende in cumulates crystallized from andesitic magmas (Erdman et al., 2016) indicates the importance of hornblende in the evolution of intermediate magmas. It is also possible that granitoids form by partial melting of amphibolites, which would also generate melts with low Ge/Si if amphibole is residual. Published

Table 3
The Mineral Modes, Ge/Si Ratio, and Ge and Si Contents of Some Representative Granitoids

	Modal Abundances in granitoids (%)							
	Qtz	Hb	Bt	Pl	Kfs	SiO_2 (wt. %)	Ge (ppm)	Ge/Si (×10^{-6})
Granite	50	2	2	30	16	81	0.87	2.29
Granodiorite	30	5	3	44	18	72.8	1.09	3.20
Monzonite	4	0	8	50	38	63.6	1.2	4.04
Diorite	5	40	5	50	0	55.6	2.42	9.29

Note. The mineral modes are assumed from Le Maitre (2002).

granitoid data (Ayuso et al., 2009; Kamei & Takagi, 2003) are in agreement with the modeled data (Figure 5). An important conclusion from our granitoid data is that the extreme differentiation (Lee & Morton, 2015) needed to generate rhyolites and granites can result in low Ge/Si, consistent with quartz having the lowest Ge/Si of all relevant silicate minerals. We note, however, that assimilation of sediments could influence Ge/Si as described below.

4.5. Implications and Unanswered Questions

In summary, we show that Ge/Si ratios and Ge/Si ratio exchange coefficients vary greatly from mineral to mineral (Table 1). Only in the case of melting peridotitic mantle and early differentiation of primitive basalt does Ge/Si remain relatively unfractionated. Garnet, amphibole, and biotite fractionation should lead to residual liquids with low Ge/Si. Quartz has the lowest Ge/Si of all magmatic minerals. A number of implications and questions follow.

First, chemical and physical weathering could enhance Ge/Si fractionation. Quartz- and feldspar-rich sands would be expected to have low Ge/Si. Clay-rich sediments, derived from micas or the breakdown of feldspars and amphiboles, will have high Ge/Si (Lugolobi et al., 2010). Basalts contaminated by sandstones might be expected to evolve toward low Ge/Si (and high Si), whereas basalts contaminated by shales might be expected to evolve to high Ge/Si (without an increase in Si; Derry et al., 2006; Iacono-Marziano et al., 2009; Kurtz et al., 2002). Our analysis of a limited data set for granitoids is undoubtedly too simplistic as contamination and crustal melting will likely complicate interpretation of Ge/Si. However, our preliminary results here provide good motivation for investigating Ge/Si systematics of more granitoids.

Ge/Si may also be helpful in distinguishing garnet from hornblende fractionation. Both garnet and hornblende are important mineral phase of the magma source of trondhjemites, tonalites, and granodiorites (Rapp et al., 1991). They are also major fractionation phases in the roots of island arcs, generating Si-rich liquids that resemble the andesitic composition of continental crust (Alonso-Perez et al., 2008; Davidson et al., 2007; Erdman et al., 2016; Lee et al., 2006; Lee et al., 2007). Separating the effects of garnet and hornblende is often difficult because heavy rare earth elements, which are typically used to quantify the influence of garnet are compatible in both garnet and hornblende. In detail, heavy rare earths are more compatible in garnet than in hornblende, so residual magmas with low heavy rare earth abundances could have had their rare earth systematics generated by small amounts of garnet fractionation or large amounts of hornblende fractionation. What makes Ge/Si systematics interesting is that the Ge/Si exchange coefficient of hornblende is 1.6 times higher than that of garnet. Thus, the combination of heavy rare earth element and Ge/Si systematics could yield an additional constraint on the involvement of hornblende or garnet in the magma source or crystallizing phases. This would complement work on the use of middle and heavy rare earths to distinguish between garnet and hornblende (Davidson et al., 2012). There is, however, not enough granitoid Ge/Si data in the literature to apply this test right now.

An unanswered question of this study is whether accessory minerals can modify Ge/Si systematics. For example, could the low Ge/Si ratios of evolved magmas, which we attribute to hornblende here be controlled by the fractionation of other phases, such as magnetite, sulfide, and apatite? Examination of Ge/Si in back-arc basin basalts (Jenner et al., 2015) shows that Ge/Si decreases at ~4 wt. % MgO, coinciding with the onset of magnetite, sulfide, apatite, and plagioclase fractionation (Figure 6). Our study here suggests plagioclase fractionation by itself should lead to an increase in Ge/Si. For Ge/Si to decrease by fractionation of the other minerals, which are in low abundance, Ge must be highly compatible in such minerals. More work is necessary to quantify the Ge systematics of magnetite and sulfide. However, the fact the Ge concentration itself does not decrease at the onset of magnetite saturation (Figure 6) suggests that these accessory phases do not play a significant role. Instead, we see that the decrease in Ge/Si is associated with an increase in SiO_2 content (Figure 6). One possibility is hornblende fractionation at depth, but these back-arc basin basalts are not known to have hornblende. We are thus unable to explain the back-arc basin fractionation Ge/Si fractionation trends.

Finally, the compatibility of Ge in biotite suggests that Ge/Si systematics of ultrapotassic magmas may be useful in quantifying the role of phlogopite in the source regions of such magmas or as fractionating phase.

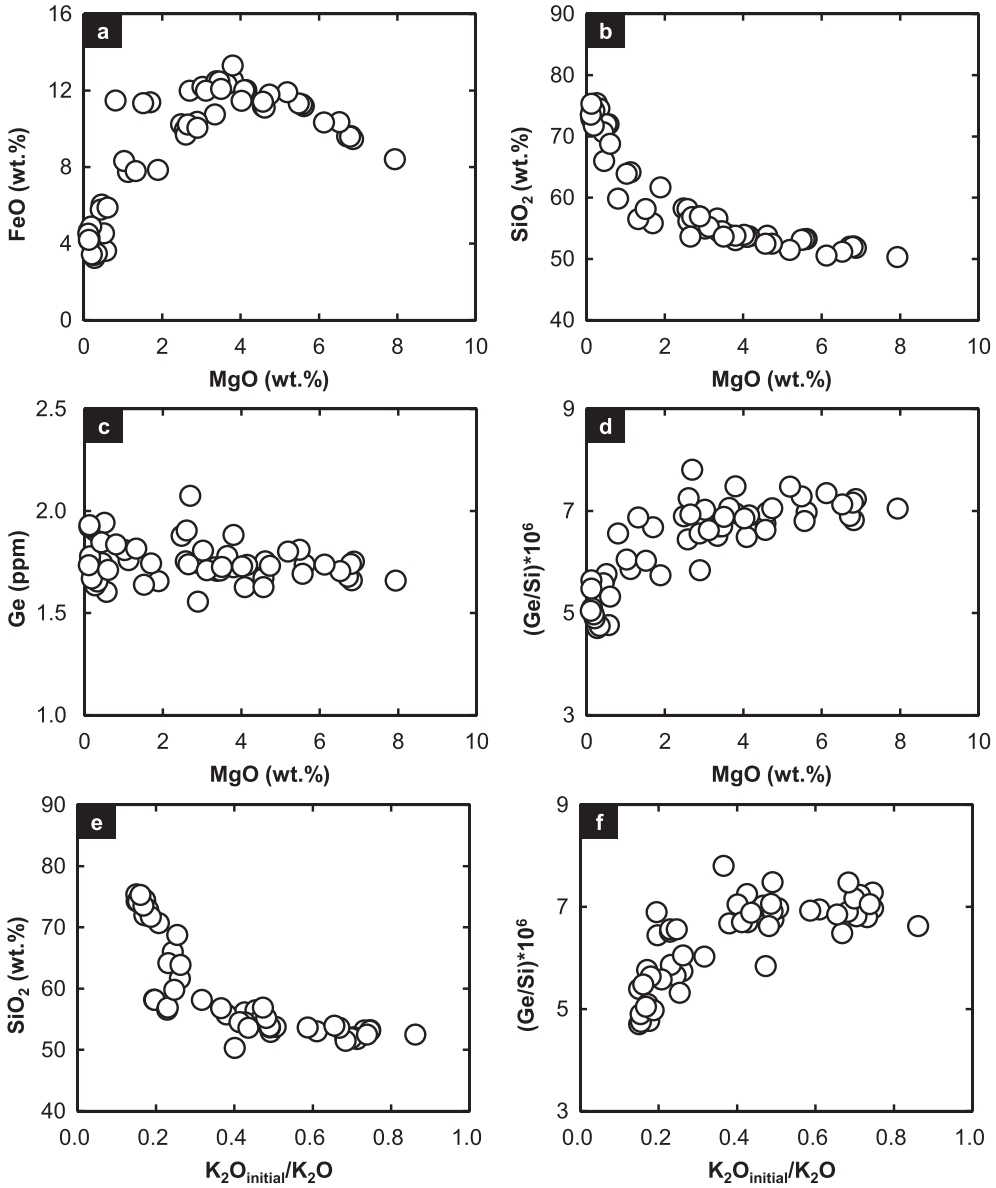

Figure 6. (a–d) FeO (wt.%), SiO_2 (wt.%), Ge (ppm), and Ge/Si ratio versus MgO (wt.%) and (e and f) SiO_2 (wt.%), Ge/Si ratio versus $K_2O_{initial}/K_2O$ for Valu Fa back-arc basins lavas in the Tonga subduction zone (Jenner et al., 2015). The $K_2O_{initial}$ is the K_2O of the lava at 8% MgO, where $K_2O_{initial}/K_2O$ is used as a proxy for residual melt fraction. Decrease in Ge/Si coincides with onset of magnetite fractionation, but magnetite fractionation does not appear to influence Ge concentration. Decrease in Ge/Si is due to an increase in SiO_2 of residual melt.

5. Conclusions

We studied the mineral/melt and intermineral exchanging behavior of Ge/Si for nine common rock-forming minerals in natural mafic and felsic systems. Ge/Si mineral/melt exchange coefficients vary by up to a factor of 10. In mafic and ultramafic systems, Ge/Si mineral/melt exchange coefficients are less than 1 for plagioclase (0.48) and olivine (0.72), close to 1 for clinopyroxene (1.17) and orthopyroxene (1.07), and greater than 1 for garnet (2.69). In felsic and silicic systems, the Ge/Si mineral/melt exchange coefficient is less than 1 for quartz (0.23), plagioclase (0.67), and potassium feldspar (0.67) but much greater than 1 for biotite (4.80) and hornblende (3.95).

The bulk peridotite/melt exchange coefficient was estimated from the measured olivine/melt exchange coefficient $K_{Ol/melt}^{Ge/Si}$ along with measured intermineral exchange coefficients, mineral modes in peridotite, and Si

contents of each phase. Over the range of typical fertile upper mantle peridotite compositions, the bulk peridotite/melt Ge/Si exchange coefficients are near unity (0.93–1.11), indicating that the Ge/Si ratio of mantle-derived melts must be similar to that of the mantle. We show that early olivine-dominated fractionation of basalts also does not lead to significant Ge/Si fractionation. However, precipitation of plagioclase causes Ge/Si to rise slightly in the residual magma.

In contrast, fractionation of hydrous magmas, where hornblende may be a major fractionating phase in more intermediate systems, the compatibility of Ge in hornblende causes residual liquids to decrease in Ge/Si. This is why granites have Ge/Si significantly lower than basalts and even the mantle.

Finally, we suggest that Ge/Si systematics may be useful in distinguishing between the effects of garnet and amphibole on the evolution of intermediate magmas in continental arcs. However, there is still insufficient bulk rock Ge data on arc magmatic rocks to pursue this direction now. And the high compatibility of Ge in micas suggests that Ge/Si systematics may also be useful in quantifying the role of phlogopite in the source regions of such magmas or as fractionating phase.

Acknowledgments
This research is cosupported by the National Science Foundation of China (41703015) and U.S. National Science Foundation grant (OCE-1338842). All analysis data can be found in EarthChem Library (doi:10.1594/IEDA/111377). We thank F. Jenner, M. Brounce, M. Humayun, and Ray Macdonald for thorough reviews and for suggestions that significantly improved the manuscript.

References

Allègre, C. J., & Turcotte, D. L. (1986). Implications of a two-component marble-cake mantle. *Nature*, *323*(6084), 123–127. https://doi.org/10.1038/323123a0

Alonso-Perez, R., Müntener, O., & Ulmer, P. (2008). Igneous garnet and amphibole fractionation in the roots of island arcs: Experimental constraints on andesitic liquids. *Contributions to Mineralogy and Petrology*, *157*(4), 541–558.

Anders, A. M., Sletten, R. S., Derry, L. A., & Hallet, B. (2003). Germanium/silicon ratios in the Copper River Basin, Alaska: Weathering and partitioning in periglacial versus glacial environments. *Journal of Geophysical Research*, *108*(F1), 6005. https://doi.org/10.1029/2003JF000026

Arevalo, R. Jr., McDonough, W. F., & Piccoli, P. M. (2011). In situ determination of first-row transition metal, Ga and Ge abundances in geological materials via medium-resolution LA-ICP-MS. *Geostandards and Geoanalytical Research*, *35*(2), 253–273. https://doi.org/10.1111/j.1751-908X.2010.00099.x

Asimow, P. D., & Ghiorso, M. S. (1998). Algorithmic modifications extending MELTS to calculate subsolidus phase relations. *American Mineralogist*, *83*(9-10), 1127–1132. https://doi.org/10.2138/am-1998-9-1022

Ayuso, R. A., Haeussler, P. J., Bradley, D. C., Farris, D. W., Foley, N. K., & Wandless, G. A. (2009). The role of ridge subduction in determining the geochemistry and Nd–Sr–Pb isotopic evolution of the Kodiak batholith in southern Alaska. *Tectonophysics*, *464*(1-4), 137–163. https://doi.org/10.1016/j.tecto.2008.09.029

Bareille, G., Labracherie, M., Mortlock, R. A., Maier-Reimer, E., & Froelich, P. N. (1998). A test of (Ge/Si)opal as a paleorecorder of (Ge/Si) seawater. *Geology*, *26*(2), 179–182. https://doi.org/10.1130/0091-7613(1998)026<0179:ATOGSO>2.3.CO;2

Beattie, P., Ford, C., & Russell, D. (1991). Partition coefficients for olivine-melt and orthopyroxene-melt systems. *Contributions to Mineralogy and Petrology*, *109*(2), 212–224. https://doi.org/10.1007/BF00306480

Bernstein, L. R. (1985). Germanium geochemistry and mineralogy. *Geochimica et Cosmochimica Acta*, *49*(11), 2409–2422. https://doi.org/10.1016/0016-7037(85)90241-8

Breiter, K., Gardenova, N., Vaculovic, T., & Kanicky, V. (2013). Topaz as an important host for Ge in granites and greisens. *Mineralogical Magazine*, *77*(4), 403–417. https://doi.org/10.1180/minmag.2013.077.4.01

Burton, J. D., Culkin, F., & Riley, J. P. (1959). The abundances of gallium and germanium in terrestrial materials. *Geochimica et Cosmochimica Acta*, *16*(1-3), 151–180. https://doi.org/10.1016/0016-7037(59)90052-3

Capobianco, C. J., & Watson, E. B. (1982). Olivine/silicate melt partitioning of germanium: An example of a nearly constant partition coefficient. *Geochimica et Cosmochimica Acta*, *46*(2), 235–240. https://doi.org/10.1016/0016-7037(82)90250-2

Chin, E. J., Lee, C.-T. A., & Barnes, J. D. (2014). Thickening, refertilization, and the deep lithosphere filter in continental arcs: Constraints from major and trace elements and oxygen isotopes. *Earth and Planetary Science Letters*, *397*, 184–200. https://doi.org/10.1016/j.epsl.2014.04.022

Dasgupta, R., Jackson, M. G., & Lee, C.-T. A. (2010). Major element chemistry of ocean island basalts—Conditions of mantle melting and heterogeneity of mantle source. *Earth and Planetary Science Letters*, *289*(3-4), 377–392. https://doi.org/10.1016/j.epsl.2009.11.027

Davidson, J., Turner, S., Handley, H., Macpherson, C., & Dosseto, A. (2007). Amphibole "sponge" in arc crust? *Geology*, *35*(9), 787. https://doi.org/10.1130/G23637A.1

Davidson, J., Turner, S., & Plank, T. (2012). Dy/Dy*: Variations arising from mantle sources and petrogenetic processes. *Journal of Petrology*, *54*(3), 525–537.

Davis, F. A., Humayun, M., Hirschmann, M. M., & Cooper, R. S. (2013). Experimentally determined mineral/melt partitioning of first-row transition elements (FRTE) during partial melting of peridotite at 3GPa. *Geochimica et Cosmochimica Acta*, *104*, 232–260. https://doi.org/10.1016/j.gca.2012.11.009

De Argollo, R., & Schilling, J. G. (1978a). Ge-Si and Ga-Al fractionation in Hawaiian volcanic rocks. *Geochimica et Cosmochimica Acta*, *42*(6), 623–630. https://doi.org/10.1016/0016-7037(78)90007-8

De Argollo, R., & Schilling, J. G. (1978b). Ge/Si and Ga/Al variations along the Reykjanes Ridge and Iceland. *Nature*, *276*(5683), 24–28. https://doi.org/10.1038/276024a0

Derry, L. A., Pett-Ridge, J. C., Kurtz, A. C., & Troester, J. W. (2006). Ge/Si and $^{87}Sr/^{86}Sr$ tracers of weathering reactions and hydrologic pathways in a tropical granitoid system. *Journal of Geochemical Exploration*, *88*(1-3), 271–274. https://doi.org/10.1016/j.gexplo.2005.08.054

Dong, L., Shen, B., Lee, C. T. A., Shu, X. J., Peng, Y., Sun, Y., et al. (2015). Germanium/silicon of the Ediacaran-Cambrian Laobao cherts: Implications for the bedded chert formation and paleoenvironment interpretations. *Geochemistry, Geophysics, Geosystems*, *16*, 751–763. https://doi.org/10.1002/2014GC005595

Erdman, M. E., Lee, C.-T. A., Levander, A., & Jiang, H. (2016). Role of arc magmatism and lower crustal foundering in controlling elevation history of the Nevadaplano and Colorado Plateau: A case study of pyroxenitic lower crust from central Arizona, USA. *Earth and Planetary Science Letters*, *439*, 48–57. https://doi.org/10.1016/j.epsl.2016.01.032

Farner, M. J., Lee, C.-T. A., & Putirka, K. D. (2014). Mafic–felsic magma mixing limited by reactive processes: A case study of biotite-rich rinds on mafic enclaves. *Earth and Planetary Science Letters*, *393*, 49–59. https://doi.org/10.1016/j.epsl.2014.02.040

Gao, S., Liu, X., Yuan, H., Hattendorf, B., Günther, D., Chen, L., & Hu, S. (2002). Determination of forty two major and trace elements in USGS and NIST SRM glasses by laser ablation-inductively coupled plasma-mass spectrometry. *Geostandards Newsletter*, *26*(2), 181–196. https://doi.org/10.1111/j.1751-908X.2002.tb00886.x

Ghiorso, M. S., Hirschmann, M. M., Reiners, P. W., & Kress, V. C. (2002). The pMELTS: A revision of MELTS for improved calculation of phase relations and major element partitioning related to partial melting of the mantle to 3 GPa. *Geochemistry, Geophysics, Geosystems*, *3*(5), 1030. https://doi.org/10.1029/2001GC000217

Ghiorso, M. S., & Sack, R. O. (1995). Chemical mass transfer in magmatic processes IV. A revised and internally consistent thermodynamic model for the interpolation and extrapolation of liquid-solid equilibria in magmatic systems at elevated temperatures and pressures. *Contributions to Mineralogy and Petrology*, *119*(2-3), 197–212.

Hammond, D. E., McManus, J., & Berelson, W. M. (2004). Oceanic germanium/silicon ratios: Evaluation of the potential overprint of temperature on weathering signals. *Paleoceanography*, *19*, PA2016. https://doi.org/10.1029/2003PA000940

Hirschmann, M. M., Kogiso, T., Baker, M. B., & Stolper, E. M. (2003). Alkalic magmas generated by partial melting of garnet pyroxenite. *Geology*, *31*(6), 481. https://doi.org/10.1130/0091-7613(2003)031<0481:AMGBPM>2.0.CO;2

Höll, R., Kling, M., & Schroll, E. (2007). Metallogenesis of germanium—A review. *Ore Geology Reviews*, *30*(3-4), 145–180. https://doi.org/10.1016/j.oregeorev.2005.07.034

Huang, S., & Humayun, M. (2016). Petrogenesis of high-CaO lavas from Mauna Kea, Hawaii: Constraints from trace element abundances. *Geochimica et Cosmochimica Acta*, *185*, 198–215.

Iacono-Marziano, G., Gaillard, F., Scaillet, B., Pichavant, M., & Chiodini, G. (2009). Role of non-mantle CO_2 in the dynamics of volcano degassing: The Mount Vesuvius example. *Geology*, *37*(4), 319–322. https://doi.org/10.1130/G25446A.1

Jenner, F. E., Hauri, E. H., Bullock, E. S., König, S., Arculus, R. J., Mavrogenes, J. A., et al. (2015). The competing effects of sulfide saturation versus degassing on the behavior of the chalcophile elements during the differentiation of hydrous melts. *Geochemistry, Geophysics, Geosystems*, *16*, 1490–1507. https://doi.org/10.1002/2014GC005670

Jenner, F. E., & O'Neill, H. S. C. (2012). Analysis of 60 elements in 616 ocean floor basaltic glasses. *Geochemistry, Geophysics, Geosystems*, *13*, Q02005. https://doi.org/10.1029/2011GC004009

Kamei, A., & Takagi, T. (2003). Geology and petrography of the Abukuma granites in the Funehiki area, Fukushima Prefecture, NE Japan. *The Journal of the Geological Society of Japan*, *109*(4), 234–251. https://doi.org/10.5575/geosoc.109.234

Kegler, P., & Holzheid, A. (2011). Determination of the formal Ge-oxide species in silicate melts at oxygen fugacities applicable to terrestrial core formation scenarios. *European Journal of Mineralogy*, *23*(3), 369–378. https://doi.org/10.1127/0935-1221/2011/0023-2097

Kurtz, A. C., Derry, L. A., & Chadwick, O. A. (2002). Germanium-silicon fractionation in the weathering environment. *Geochimica et Cosmochimica Acta*, *66*(9), 1525–1537. https://doi.org/10.1016/S0016-7037(01)00869-9

Le Maitre, R. W. (2002). *Igneous rocks: A classification and glossary of terms: Recommendations of the International Union of Geological Sciences, Subcommission on the Systematics of Igneous Rocks*. Cambridge: Cambridge University Press. https://doi.org/10.1017/CBO9780511535581

Le Maitre, R. W., Streckeisen, A., Zanettin, B., Le Bas, M., Bonin, B., & Bateman, P. (2002). *Igneous rocks: Aa classification and glossary of terms: Recommendations of the International Union of Geological Sciences Subcommission on the Systematics of Igneous Rocks*. Cambridge: Cambridge University Press.

Le Roux, V., Dasgupta, R., & Lee, C. T. A. (2011). Mineralogical heterogeneities in the Earth's mantle: Constraints from Mn, Co, Ni and Zn partitioning during partial melting. *Earth and Planetary Science Letters*, *307*(3-4), 395–408. https://doi.org/10.1016/j.epsl.2011.05.014

Le Roux, V., Dasgupta, R., & Lee, C. T. A. (2015). Recommended mineral-melt partition coefficients for FRTEs (Cu), Ga, and Ge during mantle melting. *American Mineralogist*, *100*(11-12), 2533–2544. https://doi.org/10.2138/am-2015-5215

Le Roux, V., Lee, C. T. A., & Turner, S. J. (2010). Zn/Fe systematics in mafic and ultramafic systems: Implications for detecting major element heterogeneities in the Earth's mantle. *Geochimica et Cosmochimica Acta*, *74*(9), 2779–2796. https://doi.org/10.1016/j.gca.2010.02.004

Lee, C., Rudnick, R. L., & Brimhall, G. H. (2001). Deep lithospheric dynamics beneath the Sierra Nevada during the Mesozoic and Cenozoic as inferred from xenolith petrology. *Geochemistry, Geophysics, Geosystems*, *2*(12). https://doi.org/10.1029/2001GC000152

Lee, C. T., Luffi, P., Chin, E. J., Bouchet, R., Dasgupta, R., Morton, D. M., et al. (2012). Copper systematics in arc magmas and implications for crust-mantle differentiation. *Science*, *336*(6077), 64–68. https://doi.org/10.1126/science.1217313

Lee, C. T. A., Cheng, X., & Horodyskyj, U. (2006). The development and refinement of continental arcs by primary basaltic magmatism, garnet pyroxenite accumulation, basaltic recharge and delamination: Insights from the Sierra Nevada, California. *Contributions to Mineralogy and Petrology*, *151*(2), 222–242. https://doi.org/10.1007/s00410-005-0056-1

Lee, C.-T. A., & Morton, D. M. (2015). High silica granites: Terminal porosity and crystal settling in shallow magma chambers. *Earth and Planetary Science Letters*, *409*, 23–31. https://doi.org/10.1016/j.epsl.2014.10.040

Lee, C.-T. A., Morton, D. M., Kistler, R. W., & Baird, A. K. (2007). Petrology and tectonics of Phanerozoic continent formation: From island arcs to accretion and continental arc magmatism. *Earth and Planetary Science Letters*, *263*(3-4), 370–387. https://doi.org/10.1016/j.epsl.2007.09.025

Lee, C. T. A., Oka, M., Luffi, P., & Agranier, A. (2008). Internal distribution of Li and B in serpentinites from the Feather River Ophiolite, California, based on laser ablation inductively coupled plasma mass spectrometry. *Geochemistry, Geophysics, Geosystems*, *9*, Q12011. https://doi.org/10.1029/2008GC002078

Liao, K. Z., Morton, D. M., & Lee, C.-T. A. (2013). Geochemical diagnostics of metasedimentary dark enclaves: A case study from the Peninsular Ranges Batholith, southern California. *International Geology Review*, *55*(9), 1049–1072. https://doi.org/10.1080/00206814.2012.753684

Liu, X., Xiong, X., Audétat, A., Li, Y., Song, M., Li, L., et al. (2014). Partitioning of copper between olivine, orthopyroxene, clinopyroxene, spinel, garnet and silicate melts at upper mantle conditions. *Geochimica et Cosmochimica Acta*, *125*, 1–22. https://doi.org/10.1016/j.gca.2013.09.039

Liu, Y. S., Hu, Z. C., Gao, S., Günther, D., Xu, J., Gao, C. G., & Chen, H. H. (2008). In situ analysis of major and trace elements of anhydrous minerals by LA-ICP-MS without applying an internal standard. *Chemical Geology*, *257*(1-2), 34–43. https://doi.org/10.1016/j.chemgeo.2008.08.004

Lugolobi, F., Kurtz, A. C., & Derry, L. A. (2010). Germanium–silicon fractionation in a tropical, granitic weathering environment. *Geochimica et Cosmochimica Acta*, *74*(4), 1294–1308. https://doi.org/10.1016/j.gca.2009.11.027

Macdonald, R., Rogers, N. W., & Tindle, A. G. (2007). Distribution of germanium between phenocrysts and melt in peralkaline rhyolites from the Kenya Rift Valley. *Mineralogical Magazine*, *71*(06), 703–713. https://doi.org/10.1180/minmag.2007.071.6.703

Malvin, D. J., & Drake, M. J. (1987). Experimental determination of crystal/melt partitioning of Ga and Ge in the system forsterite-anorthite-diopside. *Geochimica et Cosmochimica Acta*, *51*(8), 2117–2128. https://doi.org/10.1016/0016-7037(87)90260-2

McDonough, W. F., & Sun, S. S. (1995). The composition of the earth. *Chemical Geology*, *120*(3-4), 223–253. https://doi.org/10.1016/0009-2541(94)00140-4

Palme, H., & O'Neill, H. S. C. (2014). 3.1—Cosmochemical estimates of mantle composition. In H. D. H. K. Turekian (Ed.), *Treatise on geochemistry* (2nd ed., pp. 1–39). Oxford: Elsevier.

Pearson, D. G., Canil, D., & Shirey, S. B. (2014). 3.5—Mantle samples included in volcanic rocks: Xenoliths and diamonds. In H. D. H. K. Turekian (Ed.), *Treatise on Geochemistry* (2nd ed., pp. 169–253). Oxford: Elsevier. https://doi.org/10.1016/B978-0-08-095975-7.00216-3

Rapp, R. P., Watson, E. B., & Miller, C. F. (1991). Partial melting of amphibolite/eclogite and the origin of Archean trondhjemites and tonalites. *Precambrian Research*, *51*(1-4), 1–25. https://doi.org/10.1016/0301-9268(91)90092-O

Righter, K., King, C., Danielson, L., Pando, K., & Lee, C. T. (2011). Experimental determination of the metal/silicate partition coefficient of Germanium: Implications for core and mantle differentiation. *Earth and Planetary Science Letters*, *304*(3-4), 379–388. https://doi.org/10.1016/j.epsl.2011.02.015

Ringwood, A. E. (1955). The principles governing trace element distribution during magmatic crystallization Part I: The influence of electronegativity. *Geochimica et Cosmochimica Acta*, *7*(3-4), 189–202. https://doi.org/10.1016/0016-7037(55)90029-6

Rudnick, R. L., & Gao, S. (2003). 3.01—Composition of the continental crust. In H. D. Holland & K. K. Turekian (Eds.), *Treatise on geochemistry* (pp. 1–64). Oxford: Pergamon.

Shen, B., Lee, C.-T. A., & Xiao, S. (2011). Germanium/silica ratios in diagenetic chert nodules from the Ediacaran Doushantuo Formation, South China. *Chemical Geology*, *280*(3-4), 323–335. https://doi.org/10.1016/j.chemgeo.2010.11.019

Shu, X.-J., & Lee, C.-T. A. (2015). Sulfur determination by laser ablation high resolution magnetic sector ICP-MS applied to glasses, aphyric lavas, and micro-laminated sediments. *Chinese Journal of Geochemistry*, *34*(3), 273–288. https://doi.org/10.1007/s11631-015-0051-9

Sobolev, A. V., Hofmann, A. W., Kuzmin, D. V., Yaxley, G. M., Arndt, N. T., Chung, S. L., et al. (2007). The amount of recycled crust in sources of mantle-derived melts. *Science*, *316*(5823), 412–417. https://doi.org/10.1126/science.1138113

Tribovillard, N., Bout-Roumazeilles, V., Riboulleau, A., Baudin, F., Danelian, T., & Riquier, L. (2011). Transfer of germanium to marine sediments: Insights from its accumulation in radiolarites and authigenic capture under reducing conditions. Some examples through geological ages. *Chemical Geology*, *282*(3-4), 120–130.

Van Kooten, G. K. (1980). Mineralogy, petrology, and geochemistry of an ultrapotassic basaltic suite, Central Sierra Nevada, California, U.S. A. *Journal of Petrology*, *21*(4), 651–684. https://doi.org/10.1093/petrology/21.4.651

Walter, M. J. (1998). Melting of garnet peridotite and the origin of komatiite and depleted lithosphere. *Journal of Petrology*, *39*(1), 29–60. https://doi.org/10.1093/petroj/39.1.29

Walter, M. J. (2014). 3.10—Melt extraction and compositional variability in mantle lithosphere. In H. D. H. K. Turekian (Ed.), *Treatise on geochemistry* (2nd ed., pp. 393–419). Oxford: Elsevier. https://doi.org/10.1016/B978-0-08-095975-7.00208-4

Wasson, J. T., & Baedecker, P. A. (1970). Ga, Ge, Ir and Au in lunar, terrestrial and meteoritic basalts. In A. A. Levinson (Ed.), *Geochmica et Cosmochimica Acta, Volume 1. Proceedings of the Apollo 11 Lunar Science Conference held 5-8 January, 1970 in Houston, TX. Volume 2: Chemical and Isotope Analyses*, 2, 1741–1750. New York: Pergammon Press.

Workman, R. K., & Hart, S. R. (2005). Major and trace element composition of the depleted MORB mantle (DMM). *Earth and Planetary Science Letters*, *231*(1-2), 53–72. https://doi.org/10.1016/j.epsl.2004.12.005

Yang, S., Humayun, M., Righter, K., Jefferson, G., Fields, D., & Irving, A. J. (2015). Siderophile and chalcophile element abundances in shergottites: Implications for Martian core formation. *Meteoritics & Planetary Science*, *50*(4), 691–714. https://doi.org/10.1111/maps.12384

Yang, S., Humayun, M., & Salters, V. J. M. (2018). Elemental systematics in MORB glasses from the Mid-Atlantic Ridge. *Geochemistry, Geophysics, Geosystems*, *19*, 4236–4259. https://doi.org/10.1029/2018GC007593